

Article

Structural and Quantitative Investigation of Perovskite Pore Filling in Mesoporous Metal Oxides

Shany Gamliel ^{1,2}, Inna Popov ², Bat-El Cohen ^{1,2}, Vladimir Uvarov ² and Lioz Etgar ^{1,2,*}

¹ Institute of Chemistry, Casali Center for Applied Chemistry, The Hebrew University of Jerusalem, Jerusalem 90400, Israel; shanygamliel@gmail.com (S.G.); bat-el.cohen2@mail.huji.ac.il (B.-E.C.)

² The Center of Nanoscience and Nanotechnology, The Hebrew University of Jerusalem, Jerusalem 90400, Israel; innap@savion.huji.ac.il (I.P.); vladimiru@savion.huji.ac.il (V.U.)

* Correspondence: lioz.etgar@mail.huji.ac.il; Tel./Fax: +972-2-6585325

Academic Editors: Roberto Comparelli, Lucia Curri and Marinella Striccoli

Received: 29 September 2016; Accepted: 9 November 2016; Published: 16 November 2016

Abstract: In recent years, hybrid organic–inorganic perovskite light absorbers have attracted much attention in the field of solar cells due to their optoelectronic characteristics that enable high power conversion efficiencies. Perovskite-based solar cells' efficiency has increased dramatically from 3.8% to more than 20% in just a few years, making them a promising low-cost alternative for photovoltaic applications. The deposition of perovskite into a mesoporous metal oxide is an influential factor affecting solar cell performance. Full coverage and pore filling into the porous metal oxide are important issues in the fabrication of highly-efficient mesoporous perovskite solar cells. In this work, we carry out a structural and quantitative investigation of CH₃NH₃PbI₃ pore filling deposited via sequential two-step deposition into two different mesoporous metal oxides—TiO₂ and Al₂O₃. We avoid using a hole conductor in the perovskite solar cells studied in this work to eliminate undesirable end results. Filling oxide pores with perovskite was characterized by Energy Dispersive X-ray Spectroscopy (EDS) in Transmission Electron Microscopy (TEM) on cross-sectional focused ion beam (FIB) lamellae. Complete pore filling of CH₃NH₃PbI₃ perovskite into the metal oxide pores was observed down to X-depth, showing the presence of Pb and I inside the pores. The observations reported in this work are particularly important for mesoporous Al₂O₃ perovskite solar cells, as pore filling is essential for the operation of this solar cell structure. This work presents structural and quantitative proof of complete pore filling into mesoporous perovskite-based solar cells, substantiating their high power conversion efficiency.

Keywords: pore filling; mesoporous; perovskite; STEM-TEM; XRD

1. Introduction

Hybrid organic–inorganic perovskites have recently emerged as a promising light harvester material in solar cells due to their distinctive chemical and physical properties and simple synthesis routes. Hybrid perovskites are described by the general formula ABX₃ (A = organic group, B = Pb or Sn, and X = I, Br, Cl); methylammonium iodide (CH₃NH₃I = MAI) is the most investigated organo-metal perovskite in the field of perovskite-based solar cells [1–5].

Miyasaka et al. first used MAPbI₃ in a dye-sensitized solar cell (DSSC) configuration on mesoporous TiO₂, achieving a power conversion efficiency (PCE) of 3.8% [6]. However, these cells were unstable in the liquid electrolyte and suffered from degradation. Replacement of the liquid electrolyte with a solid-hole conductor material (HTM) solved the immediate instability problem of these solar cells, and increased their PCEs to over 10% [7]. To date, a PCE of 22.1% was demonstrated for perovskite-based solar cells [8]. PCEs of 7.6% and 10.9%, respectively, were first reported for mixed halide perovskite deposited into mesoporous Al₂O₃ and TiO₂ [9], demonstrating the ability of

perovskite to efficiently transfer electrons. Therefore, perovskite-based solar cells are not restricted to mesoporous structures, and planar configuration was also demonstrated with high PCEs [10,11]. In addition, it has been shown that perovskite can be used both as a hole conductor and a light harvester, lowering the cost and simplifying the fabrication process. These HTM-free perovskite solar cells have PCEs of 10%–12.8% [12–17].

When perovskite was first introduced into solar cells, it was initially deposited via a solution process deposition technique into the mesoporous metal oxide film using a mixture of PbI_2 and $\text{CH}_3\text{NH}_3\text{I}$ in a common polar solvent. However, this technique resulted in wide variations in the performance of the photovoltaic (PV) solar cell devices due to the uncontrolled precipitation of the perovskite, which produced large morphological variations [18]. As a result, several deposition techniques have been developed for perovskite-based solar cells, including vapor deposition, vapor assisted solution process (VASP), spray deposition, and two-step deposition [19–23].

Graetzel and co-workers first introduced the two-step deposition technique in a sensitized mesoscopic perovskite solar cell [20]. In this technique, a solution of PbI_2 in dimethylformamide (DMF) was dropped and spin-coated onto the metal oxide nanoparticles (NPs) and subsequently transformed into perovskite by dipping the electrode into a solution of $\text{CH}_3\text{NH}_3\text{I}$. The two-step deposition technique produced high efficiency solar cells, demonstrated good control over the perovskite morphology, and increased reproducibility of performance [20,21].

Moreover, perovskite pore filling into the scaffold's metal oxide layer has an impact on the PV performance. Snaith et al. [24] estimated the perovskite pore filling fractions into the metal oxide layer. They have found that complete perovskite pore filling improves the electron transport rate, photovoltage, and reduces recombination rate. This finding was also supported by Wu et al. and Nanova et al., who showed the effect of the TiO_2 morphology on the PV performance [25,26].

Due to the importance of the pore filling, in this work we provide direct observation of perovskite penetration into the metal oxide pores. We performed a structural and quantitative study of perovskite pore filling into mesoporous metal oxide. Cells without HTM were investigated; the perovskite was deposited using the two-step deposition technique. The use of HTM-free solar cells eliminates the filtration of the hole conductor into the metal oxide pores and enables thorough investigation, avoiding undesirable end results. Energy dispersive X-ray spectroscopy in transmission electron microscopy (EDS-TEM), TEM, scanning electron microscopy (SEM) and X-ray diffraction (XRD) were used to investigate the pore filling. This study provides better understanding of the formation and the percolation of perovskite within the porous metal oxide.

2. Experimental

2.1. Material Synthesis

TiO_2 paste Dyesol, DSL-90-T was diluted with ethanol in 1:4 ratio by volume, then spin coated at 2000 rpm for 10 sec on top of the compact TiO_2 layer and annealed at 500 °C for 30 min. In the case of Al_2O_3 electrode, 50 nm particle size Al_2O_3 purchased from Sigma-Aldrich was diluted with isopropanol in 1:14 ratio by volume. The deposition and annealing conditions were the same as for TiO_2 .

$\text{CH}_3\text{NH}_3\text{I}$ was synthesized as described previously [27], by reacting 30 mL of methylamine (40% in methanol, TCI) and 32.3 mL of hydroiodic acid (57 wt% in water, Aldrich) in a 250 mL round bottom flask at 0 °C for 2 h with stirring. The precipitate was recovered by putting the solution on a rotavap and carefully removing the solvents at 50 °C. The yellowish raw product of methylammonium iodide ($\text{CH}_3\text{NH}_3\text{I}$) was washed with ethanol by stirring the mixture for 30 min. Then, the mixture was filtered and washed three times with diethylether. After filtration, the solid was collected and dried at 70 °C in a vacuum oven for 24 h.

2.2. Device Fabrication

SnO₂:F (FTO) conducting glass (15 Ω·cm⁻¹ Pilkington) was etched with zinc powder and HCl (37%) to obtain the desired electrode pattern. The FTO glass was then washed with ethanol, acetone, deionized water, and finally was sonicated for 15 min. A compact layer of TiO₂ (blocking layer) was then spin coated on to the FTO substrate using a solution of titanium diisopropoxidebis(acetylacetonate) (TiDIP, 75% in isopropanol, Aldrich) in ethanol and then annealed at 500 °C for 35 min. The TiO₂ solution or the Al₂O₃ solution were spin coated subsequent to TiCl₄ treatment for 30 min at 70 °C and annealing at 450 °C for 30 min.

The synthesis of the CH₃NH₃PbI₃ on the TiO₂ or Al₂O₃ surface was carried out by a two-step deposition technique. First, PbI₂ was dissolved in DMF (0.1M) and dropped onto the TiO₂ or Al₂O₃ film and spin coated, followed by annealing at 70 °C for 30 min. In the second step, the cell was dipped into methylammonium solution (0.66M). Following the dipping step, the samples were annealed at 70 °C for another 30 min. Finally, the back contact was deposited by evaporating 70 nm of gold in vacuum of 5 × 10⁻⁶ Torr.

Structure and composition of HTM-free perovskite solar cells were analyzed with scanning electron microscopy (SEM) and scanning transmission electron microscopy (STEM), both equipped with energy dispersive X-ray spectroscopy (EDS). EDS analysis was performed on top-view samples in the FEI HR SEM Sirion (FEI, Hillsboro, OR, USA) equipped with an Oxford INCA450 EDS solid state detector (Oxford Instruments NanoAnalysis, High Wycombe, UK). TEM analysis and STEM analysis were performed on cross-sectional TEM lamellae in FEI (S)TEM Tecnai F20 G² (FEI, Hillsboro, OR, USA) equipped with EDAX EDS detector (EDAX AMETEK BV, Tilburg, The Netherlands). TEM lamellae were prepared with a FEI Helios Dual Beam focused ion beam (FIB, FEI, Hillsboro, OR, USA).

2.3. X-Ray Diffraction

X-ray diffraction measurements were performed on the D8 Advance diffractometer (Bruker AXS, Karlsruhe, Germany) with a secondary graphite monochromator, two Soller slits, and a 0.2 mm receiving slit. XRD patterns within the range 3 to 75 2θ were recorded at room temperature using CuKα radiation (λ = 1.5418 Å) with the following measurement conditions: tube voltage of 40 kV, tube current of 40 mA, step-scan mode with a step size of 0.02° 2θ and counting time of 1 s/step. TOPAS-v.3 software was used for structure refinement and crystallite size calculation (TOPAS V3, General Profile and Structure Analysis Software for Powder Diffraction Data, User's Manual, Bruker AXS, Karlsruhe, Germany, 2003).

3. Results and Discussion

The structures of the discussed perovskite-based solar cells are presented in Figures 1A,B and 2B, composed of FTO-coated glass/compact TiO₂ layer/mesoporous metal oxide/CH₃NH₃PbI₃ (MAPbI₃)/Au. The penetration of perovskite into the mesopores of two metal oxides—TiO₂, and Al₂O₃—was studied with TEM on cross-sectional lamellae prepared by FIB. Cross-section TEM images of the devices are presented in Figure 1A,B. The thicknesses of metal oxides—which demonstrate high PCEs that we studied in this work—are based on our previous reports [15,28]. The current voltage curves of this study's cells are shown in Figure 2A, the hole conductor free TiO₂/ MAPbI₃ cell has V_{oc} of 0.85 V, current density (J_{sc}) of 18 mA/cm², fill factor (FF) of 56% with efficiency of 8.5%. The hole conductor free cell based on Al₂O₃/MAPbI₃ shows V_{oc} of 0.88 V, J_{sc} of 13.9 mA/cm², FF of 17%, with efficiency of 2.1%. The photovoltaic results demonstrate that both cells are working, which strengthens the discussion in this manuscript. It is important to note that these cells are hole conductor free; in particular, in the case of the Al₂O₃-based cell, the perovskite is the only charge transporter, as will be discussed below. The s-shape in the current–voltage curve for the Al₂O₃-based cell may be due to charge accumulation in this specific device structure. The exact reason is out of the scope of this work.

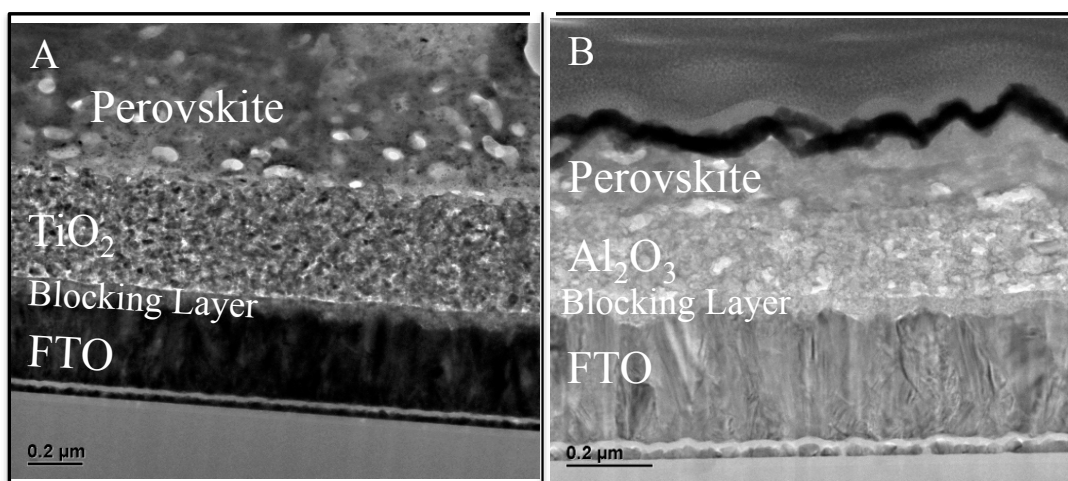


Figure 1. Transmission electron microscopy (TEM) images of cross-sectional samples prepared by focused ion beam (FIB) from (A) TiO₂/perovskite solar cell; and (B) Al₂O₃/perovskite solar cell.

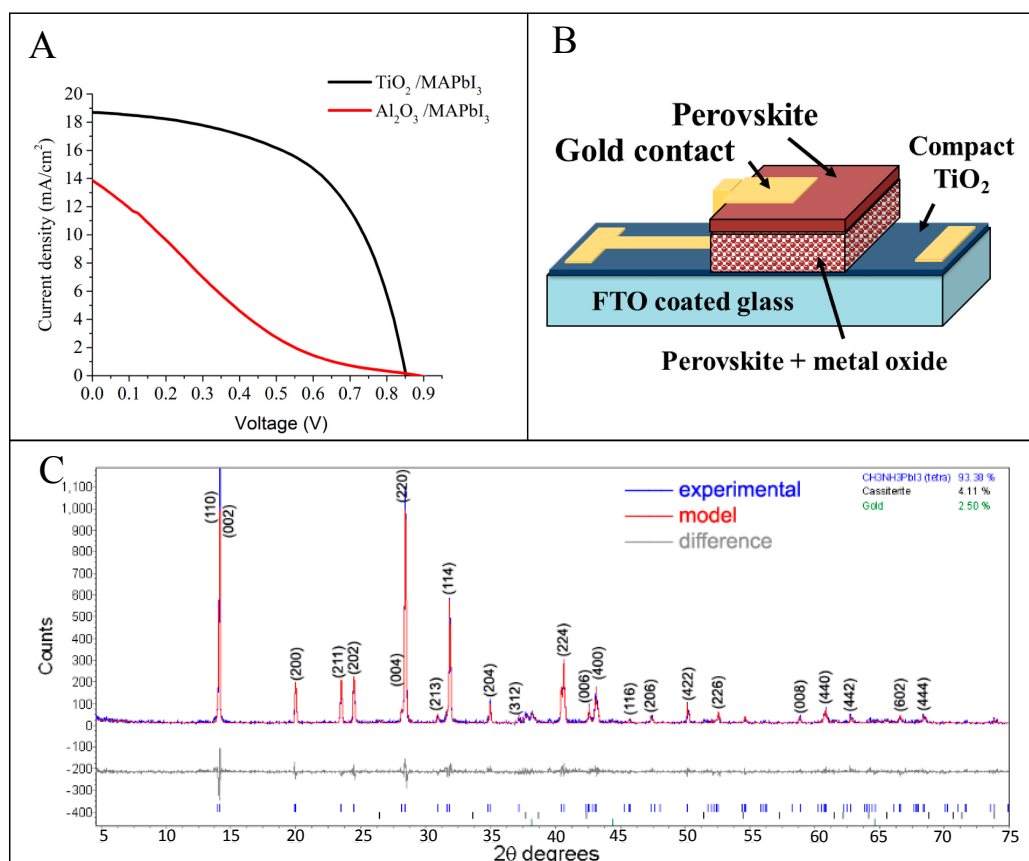


Figure 2. (A) Current–voltage curves of the study’s solar cells; (B) Schematic illustration of the solar cell; (C) Graphical representation of Rietveld refinement results. Peak positions of CH₃NH₃PbI₃, cassiterite, and gold are shown by vertical bars. FTO: SnO₂:F.

The graphical result of Rietveld refinement of XRD pattern acquired from the sample shown in Figure 3B is presented in Figure 2C. According to Rietveld refinement results, the synthesized CH₃NH₃PbI₃ has a tetragonal perovskite structure with I4/mcm space group and unit cell parameters $a = b = 8.8695(16) \text{ \AA}$, $c = 12.6532(24) \text{ \AA}$. Calculated unit cell parameters are in a good agreement with

the same reported by Lilliu et al. [29,30]. Crystallite size calculated using the Scherrer equation is equal to 356 nm. This is in a good agreement with the character of electron diffraction patterns obtained from the same sample (see Figures 5 and 6).

Elemental composition of the samples was analyzed with EDS in SEM and TEM. Figure 3A,C show the EDS spectra acquired at top-view samples of the TiO_2 /perovskite and the Al_2O_3 /perovskite solar cells in SEM. They reveal the presence of Pb, Ti, Al, O, Ca, Si, and I. Calcium and silicon signals are contributions of the FTO-coated glass. Quantitative analysis of the EDS spectra shows that the atomic ratios of Pb/I are 10:34 for TiO_2 /perovskite and 4:11 for the Al_2O_3 /perovskite solar cells. The observed ratios are very close to the value of 1:3 that indicates successful deposition of stoichiometric $\text{CH}_3\text{NH}_3\text{PbI}_3$ perovskite in both cases. Figure 3B,D show the SEM images of the areas from which EDS spectra were acquired. It is important to note that in both cases, large perovskite crystals of 100–200 nm can be observed, while in the case of the Al_2O_3 /perovskite, the coverage seems to be slightly better, although the PV performance is lower.

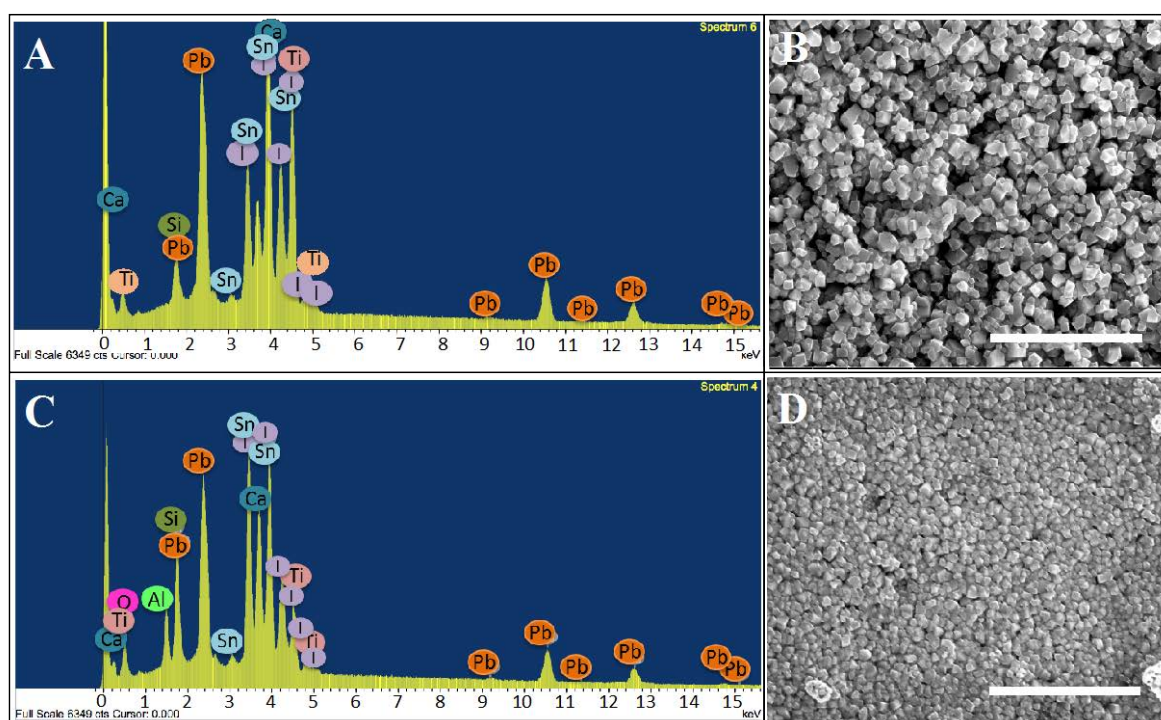


Figure 3. Energy dispersive X-ray spectroscopy (EDS) spectra acquired in scanning electron microscopy (SEM) at the top view samples of the TiO_2 /perovskite (spectrum (A) and image (B)) and the Al_2O_3 /perovskite (spectrum (C) and image (D)) solar cells. Scale bars are 5 μm .

Additional elemental analysis of the perovskite sample was done by X-ray photoelectron spectroscopy (XPS), presented in Figure 4. The XPS shows the presence of Pb, I, C, and N with a ratio of 3.6 for I/Pb—further support of the successful deposition of stoichiometric $\text{CH}_3\text{NH}_3\text{PbI}_3$ perovskite. The quantification results of the XPS analysis are provided in Table S1.

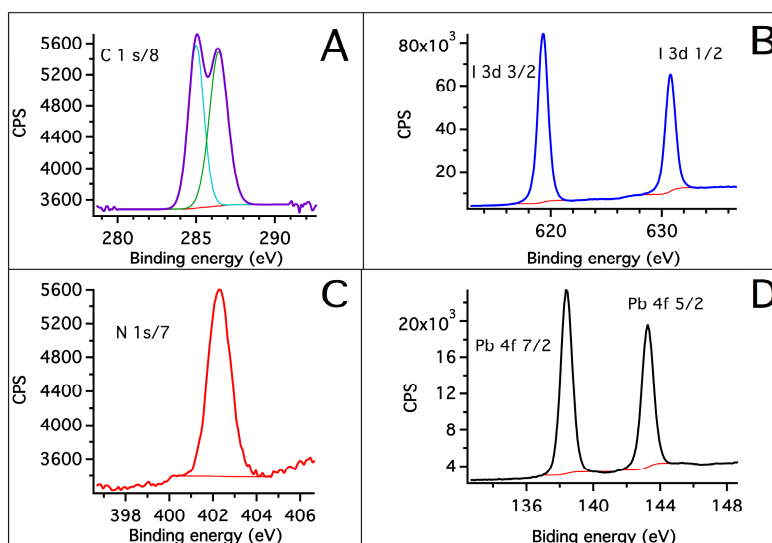


Figure 4. X-ray photoelectron spectroscopy (XPS) spectra of the perovskite sample, presenting the different elements. C1s (A), I3d 1/2 and I 3d 3/2 (B), N1s (C), Pb 4f 7/2 and Pb 4f 5/2 (D).

To investigate filling of pores by perovskite within the mesoporous metal oxides, we used STEM-based energy-dispersive X-ray (STEM-EDS) analysis. Figures 5A and 6A show the location of the EDS line scan performed in the STEM-EDS line scans of TiO_2 /perovskite and Al_2O_3 /perovskite solar cells, respectively. The line scanning started in the perovskite layer and ended deep in the metal oxide film.

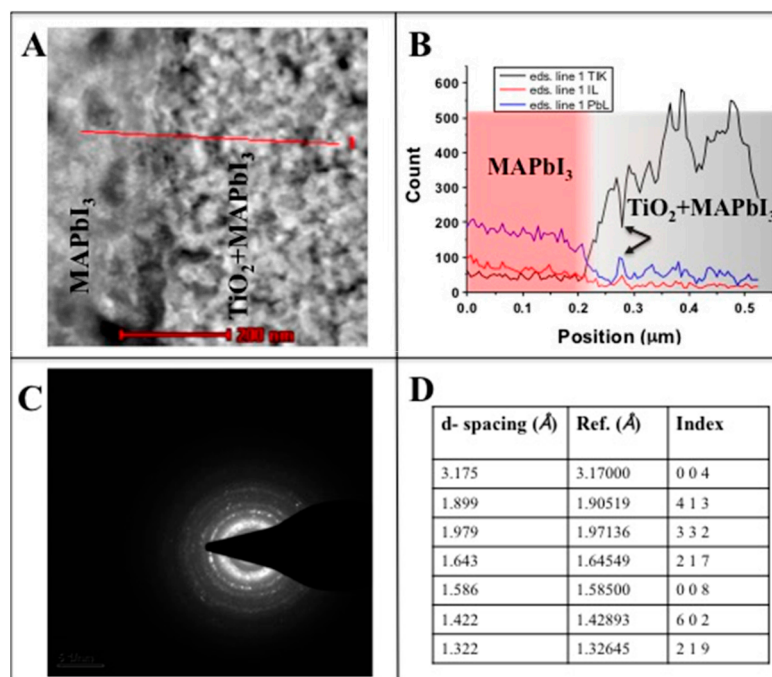


Figure 5. (A) Scanning transmission electron microscopy (STEM) image of a cross-sectioned TiO_2 /perovskite solar cell; (B) Energy dispersive X-ray spectroscopy (EDS) line profiles of PbL, IL, and TiK signals along the line shown on the STEM image; (C) Electron diffraction pattern acquired at the $\text{CH}_3\text{NH}_3\text{PbI}_3$ region; (D) d-spacing between the adjacent lattice planes measured on the pattern C.

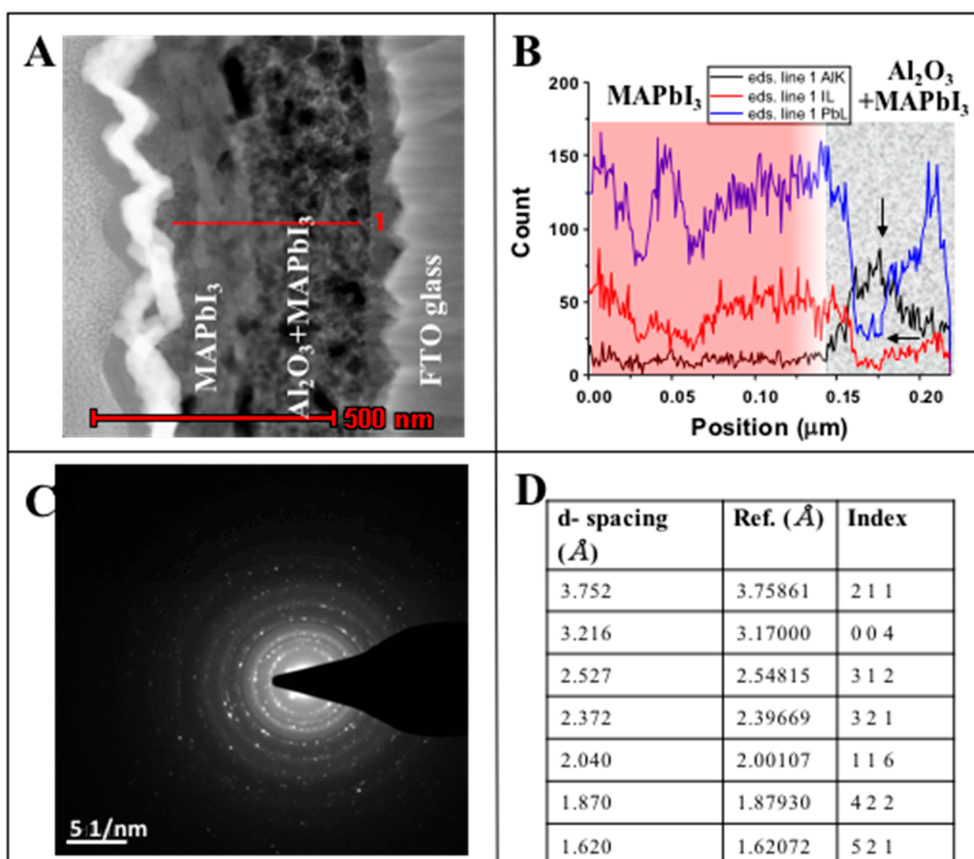


Figure 6. (A) STEM image of a cross-sectioned Al_2O_3 /perovskite solar cell; (B) EDS line profile of PbL, IL, and AlK signals along the line shown on the STEM image; (C) Electron diffraction pattern acquired at the $\text{CH}_3\text{NH}_3\text{PbI}_3$ (MAPbI_3) region; (D) d-spacing between the adjacent lattice planes measured on the pattern C.

The line profiles of elemental compositions of the two cells are shown in Figures 5B and 6B. (Figures S1 and S2 demonstrate additional STEM-EDS line scans of the two interfaces, which show the reliability of the results) The data demonstrate the presence of Pb and I throughout the perovskite and the metal oxide film, indicating that the $\text{CH}_3\text{NH}_3\text{PbI}_3$ perovskite penetrates into the metal oxide films (e.g., TiO_2 and Al_2O_3). As seen, the intensities of PbL and IL signals are higher at the perovskite layer, and decrease at the perovskite/metal oxide interface and at the metal oxide film. Simultaneously, a sharp increase in the TiK and AlK signals indicates the positions of perovskite/metal oxide interfaces in both samples. Within the metal oxide films, both TiK and AlK signals are changing following the mesoporous structure of oxides: the maxima appear at the locations of oxide grains, while the minima appear at the pores. It is worth noting that within the oxide layer, PbL and IL signals (i.e., the perovskite markers) also follow the mesoporous structure, while their signal changes are anti-phase to those of oxide markers: maxima of PbL and IL appear at pores' locations (marked with arrows for clarity in Figures 5B and 6B).

This observation is direct proof of complete filling of the oxide pores with perovskite containing both Pb and I. In particular, the complete pore filling in the case of mesoporous Al_2O_3 documents the reason why this solar cell functions successfully with scaffold layer. It was previously reported [10] that the Al_2O_3 functions as a scaffold, so that charges are transported through the perovskite, which requires a complete pore filling of the Al_2O_3 film.

Although both Pb and I were found in the perovskite and in the metal oxide layers of TEM samples, their Pb:I ratio measured within the perovskite was about 1:1. This value differs significantly from the stoichiometric value of 1:3 observed in SEM samples. We relate this phenomenon to the

preferential loss of iodine during the FIB lamella preparation (as mentioned, the samples show 1:3 ratio in the EDS-SEM analysis and high crystalline structure in the XRD spectrum, where the lamella preparation was not required). Moreover, the ratio of 1:1 for Pb:I also excludes the possibility of PbI₂ residue in the pores.

The structure of the perovskite layer was characterized by selected area electron diffraction in TEM. The patterns obtained in TiO₂ and Al₂O₃ samples are presented in Figures 5C and 6C, respectively.

The d-spacing measured on these patterns are shown in Figures 5D and 6D, along with reported structural data, which shows the crystalline tetragonal perovskite I4/mcm with unit cell parameters $a = b = 8.87 \text{ \AA}$ and $c = 12.67 \text{ \AA}$ [31–33]. Both patterns are of ring-type, which indicates the presence of a large number of randomly-oriented nanoscale crystallites in each of the perovskite layers. The strongest diffraction is observed around inter-planar spacing of 3.17–3.2 Å in both patterns, which reasonably matches the reported data for the tetragonal I4/mcm ($a = b = 8.87 \text{ \AA}$, $c = 12.67 \text{ \AA}$) perovskite [25,28,31]. However, the sets of diffraction reflexes appearing in both patterns do not coincide. Based on these two observations, we suggest that while the major part of nanocrystalline perovskite ensembles has the crystalline structure of the tetragonal perovskite, each of the analyzed perovskite layers contains “occasional” nanocrystals with different structures. We relate the observed structural features of perovskite to the ion beam damage at the sample preparation in FIB. The changes in the elemental composition observed with EDS should necessarily be accompanied by structural changes. To conclude, perovskite layers of TiO₂ and Al₂O₃ cells are structurally similar to the tetragonal perovskite, although their electron diffraction data document different stages of structural decomposition.

4. Conclusions

In this work, we performed a quantitative and structural study of hybrid perovskite pore filling into mesoporous metal oxides, TiO₂ and Al₂O₃. STEM-EDS characterization on cross-sectional FIB lamellae showed the presence of Pb and I inside the pores. SEM and XRD showed the highly crystalline structure of the tetragonal perovskite with a 1:3 ratio of Pb:I. Moreover, submicron structure of the perovskite was observed by XRD and by selected electron diffraction pattern via TEM. This work demonstrates direct proof of perovskite pore filling into mesoporous metal oxides. These results support previous assumptions about complete pore filling in mesoporous perovskite-based solar cells. The observations reported in this work are in particular important for mesoporous Al₂O₃ perovskite solar cells, as pore filling is essential for the operation of this solar cell structure.

Supplementary Materials: The following are available online at <http://www.mdpi.com/2073-4352/6/11/149/s1>: Figure S1: Scanning transmission electron microscopy (STEM) image of a cross-sectioned TiO₂/perovskite solar cell and the energy dispersive X-ray spectroscopy (EDS) line profiles of PbL, IL, and TiK signals along the line shown on the STEM image. MAPbI₃: CH₃NH₃PbI₃; Figure S2: STEM image of a cross-sectioned Al₂O₃/perovskite solar cell and the EDS line profile of PbL, IL, and AlK signals along the line shown on the STEM image; Table S1: X-ray photoelectron spectroscopy (XPS) quantification report of the perovskite sample.

Acknowledgments: We would like to acknowledge the financial support of Israel Alternative Energy Foundation (I-SAEF), the Tashtiot Project of the Office of the Chief Scientist. We would like to thank Yafit Fleger, the head of FIB unit, Institute of Nanotechnology & Advanced Materials (BINA) at Bar-Ilan University.

Author Contributions: Shany Gamliel conceived and designed the experiments; Bat-El Cohen performed the experiments; Vladimir Uvarov performed the XRD measurements, Inna Popov performed the STEM-TEM measurements and analyzed the data; Lioz Etgar planned and analyzed the experiments and wrote the manuscript.

Conflicts of Interest: The authors declare no conflict of interest.

References

1. Gratzel, M. The light and shade of perovskite solar cells. *Nat. Mater.* **2014**, *13*, 838–842. [[CrossRef](#)] [[PubMed](#)]
2. Green, M.A.; Ho-baillie, A.; Snaith, H.J. The emergence of perovskite solar cells. *Nat. Photon.* **2014**, *8*, 506–513. [[CrossRef](#)]
3. Yang, Z.; Zhang, W.-H. Organolead halide perovskite: A rising player in high-efficiency solar cells. *Chin. J. Catal.* **2014**, *35*, 983–988. [[CrossRef](#)]

4. Jung, H.S.; Park, N.-G. Perovskite Solar Cells: From Materials to Devices. *Small* **2015**, *11*, 10–25. [[CrossRef](#)] [[PubMed](#)]
5. Leijtens, T.; Eperon, G.E.; Noel, N.K.; Habisreutinger, S.N.; Petrozza, A.; Snaith, H.J. Stability of Metal Halide Perovskite Solar Cells. *Adv. Energy Mater.* **2015**, *5*. [[CrossRef](#)]
6. Kojima, A.; Teshima, K.; Shirai, Y.; Miyasaka, T. Organometal Halide Perovskites as Visible-Light Sensitizers for Photovoltaic Cells. *J. Am. Chem. Soc.* **2009**, *131*, 6050–6051. [[CrossRef](#)] [[PubMed](#)]
7. Kim, H.-S.; Lee, C.-R.; Im, J.-H.; Lee, K.-B.; Moehl, T.; Marchioro, A.; Moon, S.-J.; Baker, R.-H.; Yum, J.-H.; Moser, J.E.; et al. Lead iodide perovskite sensitized all-solid-state submicron thin film mesoscopic solar cell with efficiency exceeding 9%. *Sci. Rep.* **2012**, *2*, 591. [[CrossRef](#)] [[PubMed](#)]
8. National Renewable Energy Laboratories NREL. Available online: http://www.nrel.gov/ncpv/images/efficiency_chart.jpg (accessed on 28 October 2016).
9. Lee, M.M.; Teuscher, J.; Miyasaka, T.; Murakami, T.N.; Snaith, H.J. Efficient Hybrid Solar Cells Based on Meso-Superstructured Organometal Halide Perovskites. *Science* **2012**, *338*, 643–647. [[CrossRef](#)] [[PubMed](#)]
10. Liu, D.; Timothy, L. Kelly, perovskite solar cells with a planar heterojunction structure prepared using room-temperature solution processing techniques. *Nat. Photon.* **2014**, *8*, 133–138. [[CrossRef](#)]
11. Docampo, P.; Ball, J.M.; Darwich, M.; Eperon, G.E.; Snaith, H.J. Efficient organometaltrihalide perovskite planar-heterojunction solar cells on flexible polymer substrates. *Nat. Commun.* **2013**, *4*, 2761. [[CrossRef](#)] [[PubMed](#)]
12. Etgar, L.; Peng, G.; Xue, Z.; Liu, B.; Nazeeruddin, M.K.; Grätzel, M. Mesoscopic CH₃NH₃PbI₃/TiO₂ heterojunction solar cell. *J. Am. Chem. Soc.* **2012**, *134*, 17396–17399. [[CrossRef](#)] [[PubMed](#)]
13. Laben, W.A.; Etgar, L. Depleted hole conductor-free lead halide iodide heterojunction solar cell. *Energy Environ. Sci.* **2013**, *6*, 3249–3253. [[CrossRef](#)]
14. Aharon, S.; Gamliel, S.; Cohen, B.; Etgar, L. Depletion region effect of highly efficient hole conductor free CH₃NH₃PbI₃ perovskite solar cells. *Phys. Chem. Chem. Phys.* **2014**, *16*, 10512–10518. [[CrossRef](#)] [[PubMed](#)]
15. Cohen, B.E.; Gamliel, S.; Etgar, L. Parameters influencing the deposition of methylammonium lead halide iodide in hole conductor free perovskite-based solar cells. *Appl. Mater.* **2014**, *2*, 081502. [[CrossRef](#)]
16. Shi, J.; Dong, J.; Lv, S.; Xu, Y.; Zhu, L.; Xiao, J.; Xu, X.; Wu, H.; Li, D.; Luo, Y.; et al. Hole-conductor-free perovskite organic lead iodide heterojunction thin-film solar cells: High efficiency and junction property. *Appl. Phys. Lett.* **2014**, *104*, 063901. [[CrossRef](#)]
17. Mei, A.; Li, X.; Liu, L.; Ku, Z.; Liu, T.; Rong, Y.; Xu, M.; Hu, M.; Chen, J.; Yang, Y.; et al. A hole-conductor-free, fully printable mesoscopic perovskite solar cell with high stability. *Science* **2014**, *345*, 295–298. [[CrossRef](#)] [[PubMed](#)]
18. Liul, M.; Johnston, M.B.; Snaith, H.J. Efficient planar heterojunction perovskite solar cells by vapour deposition. *Nature* **2013**, *501*, 395–399.
19. Im, J.-H.; Jang, I.-H.; Pellet, N.; Grätzel, M.; Park, N.-G. Growth of CH₃NH₃PbI₃ cuboids with controlled size for high-efficiency perovskite solar cells. *Nat. Nanotechnol.* **2014**, *9*, 927–932. [[CrossRef](#)] [[PubMed](#)]
20. Burschka, J.; Pellet, N.; Moon, S.-J.; Humphry-Baker, R.; Gao, P.; Nazeeruddin, M.K.; Graetzel, M. Sequential deposition as a route to high-performance perovskite-sensitized solar cells. *Nature* **2013**, *499*, 316. [[CrossRef](#)] [[PubMed](#)]
21. Chen, Q.; Zhou, H.; Hong, Z.; Luo, S.; Duan, H.-S.; Wang, H.-H.; Liu, Y.; Li, G.; Yang, Y. Planar heterojunction perovskite solar cells via vapor-assisted solution process. *J. Am. Chem. Soc.* **2014**, *136*, 622–625. [[CrossRef](#)] [[PubMed](#)]
22. Barrows, A.T.; Pearson, A.J.; Kwak, C.K.; Dunbar, A.D.F.; Buckley, A.R.; Lidzey, D.G. Efficient planar heterojunction mixed-halide perovskite solar cell deposited via spray deposition. *Energy Environ. Sci.* **2014**, *7*, 2944–2950. [[CrossRef](#)]
23. Gamliel, S.; Dymshits, A.; Aharon, S.; Terkieltaub, E.; Etgar, L. Micrometer Sized Perovskite Crystals in Planar Hole Conductor Free Solar Cells. *J. Phys. Chem C* **2015**, *34*, 19722–19728. [[CrossRef](#)]
24. Leijtens, T.; Lauber, B.; Eperon, G.E.; Stranks, S.D.; Snaith, H.J. The Importance of Perovskite Pore Filling in Organometal Mixed Halide Sensitized TiO₂-Based Solar Cells. *J. Phys. Chem. Lett.* **2014**, *7*, 1096–1102. [[CrossRef](#)] [[PubMed](#)]
25. Wu, Y.; Chen, W.; Yue, Y.; Liu, J.; Bi, E.; Yang, X.; Islam, A.; Han, L. Consecutive Morphology Controlling Operations for Highly Reproducible Mesosuperstructured Perovskite Solar Cells. *ACS Appl. Mater. Interfaces* **2015**, *7*, 20707–20713. [[CrossRef](#)] [[PubMed](#)]

26. Nanova, D.; Kast, A.K.; Pfannmüller, M.; Müller, C.; Veith, L.; Wacker, I.; Agari, M.; Hermes, W.; Erk, P.; Kowalsky, W.; et al. Unraveling the Nanoscale Morphologies of Mesoporous Perovskite Solar Cells and Their Correlation to Device Performance. *Nano Lett.* **2014**, *14*, 2735–2740. [[CrossRef](#)] [[PubMed](#)]
27. Jeong, H.; Jaehoon, C.; Seung, J.K.; Nam, G.P. Synthesis, structure, and photovoltaic property of a nanocrystalline 2H perovskite-type novel sensitizer (CH₃CH₂NH₃)PbI₃. *Nanoscale Res. Lett.* **2012**, *7*, 353.
28. Dymshits, A.; Rotem, A.; Etgar, L. High voltage in hole conductor free organo metal halide perovskite solar cells. *J. Mater. Chem. A* **2014**, *2*, 20776–20781. [[CrossRef](#)]
29. Lilliu, S.; Dane, T.G.; Alsari, M.; Griffin, J.; Barrows, A.T.; Dahlem, M.S.; Friend, R.H.; Lidzey, D.G.; Macdonald, J.E. Mapping morphological and structural properties of lead halide perovskites by scanning nanofocus XRD. *Adv. Funct. Mater.* **2016**. [[CrossRef](#)]
30. Barrows, A.T.; Lilliu, S.; Pearson, A.J.; Babonneau, D.; Dunbar, A.D.F.; Lidzey, D.G. Monitoring the Formation of a CH₃NH₃PbI₃-xCl_x Perovskite during Thermal Annealing Using X-ray Scattering. *Adv. Funct. Mater.* **2016**, *26*, 4934–4942. [[CrossRef](#)]
31. Kawamura, Y.; Mashiyama, H.; Hasebe, K. Structural Study on Cubic–Tetragonal Transition of CH₃NH₃PbI₃. *J. Phys. Soc. Jpn.* **2012**, *71*, 1694–1697. [[CrossRef](#)]
32. Baikie, T.; Fang, Y.; Kadro, J.M.; Schreyer, M.; Wei, F.; Mhaisalkar, S.G.; Graetzel, M.; White, T.J. Synthesis and crystal chemistry of the hybrid perovskite (CH₃NH₃)PbI₃ for solid-state sensitized solar cell applications. *J. Mater. Chem. A* **2013**, *1*, 5628–5641. [[CrossRef](#)]
33. Im, J.-H.; Lee, C.-R.; Lee, J.-W.; Park, S.-W.; Park, N.-G. 6.5% efficient perovskite quantum-dot-sensitized solar cell. *Nanoscale* **2011**, *3*, 4088–4093. [[CrossRef](#)] [[PubMed](#)]



© 2016 by the authors; licensee MDPI, Basel, Switzerland. This article is an open access article distributed under the terms and conditions of the Creative Commons Attribution (CC-BY) license (<http://creativecommons.org/licenses/by/4.0/>).